Bridging the gap between mathematical optimization and structural engineering Design, experiments and numerical simulation of optimized concrete girders

Pressmair, Nadine; Xia, Yi; Wu, Hongfei; Langelaar, Matthijs; Hendriks, Max A.N.; Majdouba, Ahmad; Mogra, Mihir; Grisaro, Hezi; Amir, Oded; Kromoser, Benjamin

DOI
10.1002/suco.202201096

Publication date
2023

Document Version
Final published version

Published in
Structural Concrete

Citation (APA)
Pressmair, N., Xia, Y., Wu, H., Langelaar, M., Hendriks, M. A. N., Majdouba, A., Mogra, M., Grisaro, H., Amir, O., & Kromoser, B. (2023). Bridging the gap between mathematical optimization and structural engineering: Design, experiments and numerical simulation of optimized concrete girders. *Structural Concrete*, *24*(4), 5314-5330. https://doi.org/10.1002/suco.202201096

Received: 16 November 2022 | Revised: 9 February 2023 | Accepted: 21 February 2023

DOI: 10.1002/suco.202201096

ARTICLE

fib CEB-FIP WILEY

Bridging the gap between mathematical optimization and structural engineering: Design, experiments and numerical simulation of optimized concrete girders

Nadine Pressmair[1] | **Yi Xia**[2,3] | **Hongfei Wu**[2,3] | **Matthijs Langelaar**[4] | **Max A. N. Hendriks**[5,6] | **Ahmad Majdouba**[7] | **Mihir Mogra**[7] | **Hezi Grisaro**[7] | **Oded Amir**[7] | **Benjamin Kromoser**[1]

[1]Institute of Green Civil Engineering, University of Natural Resources and Life Sciences, Vienna, Austria

[2]School of Civil Engineering, Chongqing University, Chongqing, China

[3]Key Laboratory of New Technology for Construction of Cities in Mountain Area of Ministry of Education, Chongqing University, Chongqing, China

[4]Faculty of Mechanical, Maritime and Materials Engineering, Delft University of Technology, Delft, The Netherlands

[5]Faculty of Civil Engineering & Geosciences, Delft University of Technology, Delft, The Netherlands

[6]Department of Structural Engineering, Norwegian University of Science and Technology (NTNU), Trondheim, Norway

[7]Faculty of Civil and Environmental Engineering, Technion – Israel Institute of Technology, Haifa, Israel

Correspondence
Nadine Pressmair, Institute of Green Civil Engineering, University of Natural Resources and Life Sciences Vienna, Peter-Jordan-Straße 82, 1190 Vienna, Austria (formerly known as Nadine Stoiber).
Email: nadine.pressmair@boku.ac.at

Abstract

Concrete, as the most widely used construction material, is associated with a high environmental impact. Within the present study, structural optimization is the method of choice to counter this issue. The entire process, from optimization, to design, experiments and numerical simulation is outlined. Embedded in the framework of a design competition (Concrete Girder Optimization Competition 2021), a bridge between structural engineering and mathematical optimization is demonstrated. Two design concepts for optimized concrete girders, one with internal and one with external reinforcement, yet both based on strut-and-tie modeling, were investigated. Within the boundaries of the competition, several conclusions can be drawn: The results indicate the importance of an adequate structural interpretation of topology optimization results to obtain satisfying structural performance. The environmental evaluation outlines that the reinforcement mass has a substantial share in the total Global Warming Potential. A successful numerical re-simulation of selected girders can serve as a modeling base for other researchers. Compared to a conventionally designed girder an increase in resource efficiency, measured by load-carrying capacity versus environmental impact, of more than 30% was achieved.

KEYWORDS

CO_2, competition, concrete girder, concrete truss, global warming potential, lightweight design, resource efficiency, structural optimization, strut-and-tie modeling, topology optimization

Discussion on this paper must be submitted within two months of the print publication. The discussion will then be published in print, along with the authors' closure, if any, approximately nine months after the print publication.

1 | INTRODUCTION

In 2021, global CO_2 emissions from chemical and industrial processes in cement production amounted to approximately 1.7 and 1.0 Gt, respectively.[1] The sum of these two values accounts for around 7% CO_2 emission, with a steady increase observed over the last few decades. Against the backdrop of the omnipresent global climate challenges, this fact highlights the need for an enhancement of resource-efficiency within the concrete construction sector.[2,3] In this context, there are several strategies to reduce the use of cement in concrete structures while preserving performance. These include advances in material technology, manufacturing strategies as well as the optimization of the structural geometry of concrete elements,[4] with the latter being the subject of the present study.

In general, structural optimization can be divided into three disciplines: Size, shape and topology optimization. Topology optimization refers to the ideal arrangement of material within a given design space and has been increasingly taken up in structural concrete research since the turn of the millennium, as discussed by Stoiber and Kromoser.[5] The optimization of reinforced concrete structures can be further roughly divided into an optimization of the reinforcement layout or an optimization of the concrete domain. In this context, structural optimization tools are frequently consulted to generate strut-and-tie models as a guidance for structural concrete design.[6–8] These aim at representing the flow of forces within a concrete structure as accurately as possible and, thus allow the definition of reinforcement arrangements and concrete body geometries that maximize the exploitation of the used materials' strength and stiffness properties. In recent years, environmental parameters have also been increasingly taken into account within a structural optimization process. The study of Mergos,[9] intending to minimize the CO_2 of reinforced concrete structures designed against earthquake hazard via a consultation of mathematical optimization methods, can be named as one possible example. On a different note, Zhang and Zhang[10] employ a multi-objective genetic algorithm to optimize embodied emissions as well as costs in structures with the goal of identifying the key parameters, as for example cross-sectional dimensions or material properties that contribute to sustainable design.

In order to evaluate the different approaches to enhancing the resource efficiency in concrete construction fairly, practical implementation and feasibility of optimized concrete structures needs to be looked into in addition to pure numerical studies. Smarslik and Mark[11] present an experimental study on structurally optimized concrete girders with an innovative reinforcement concept based on a hybrid truss-continuum topology optimization to improve the structural performance of longitudinal joints in tunnel lining elements. As suggested by the results, an increase of the carrying capacity by 20% to 40% could be achieved. Other than that, the design, fabrication and experimental investigation of an optimized reinforced concrete truss structure as well as of a hybrid concrete-steel truss structure are presented by Gagaenlis and Mark.[12] In their case, the application of topology optimization enabled a weight reduction of more than 50% while preserving the original load-carrying and stiffness behavior. Unfortunately, the practical approach of the two above-mentioned studies does not reflect the majority of scientific activities, as a predominant emphasis on numerical investigations is identified for the case of topology optimized concrete structures by Stoiber and Kromoser.[5] To contribute to the practical investigations on structurally optimized concrete girders, the authors from the University of Natural Resources and Life Sciences in Vienna decided to host a Concrete Girder Optimization Competition 2021, where optimized designs within given span, load and material boundary conditions aiming at a minimal environmental impact were submitted by the participants and the testing as well as the evaluation of the structural performance was done by the hosting institution. The competition would serve as showcase for successful collaboration between civil engineers and mathematicians, with the latter being experts in the field of optimization and the former in the field of implementation and realization of concrete structures. To the authors' knowledge, a competition of this kind had not been carried out before, as similar competitions in the field of structural concrete mostly focused on the numerical prediction of experimental results. Galmarini et al.,[13] for example, performed tests on reinforced concrete slab strips under axial tension and transverse load at the ETH Zurich in 2012. The competition unveiled the challenge of predicting results for cracked concrete, with failure modes and deflection being generally underestimated by the participants. Another competition with comparable findings is outlined by Barros et al.,[14] where the performance of steel fiber-reinforced T-beams, failing in shear, had to be predicted.

In the following, the structure of the presented study is briefly outlined. After the introduction, the framework of the competition is explained, followed by a presentation of the two optimization, design and structural detailing strategies. The methodology of the experiments is outlined and the results are illustrated. Five girder specimens were tested in total, with two based on the design concept of submitter group A, two on the proposal of submitter group B and one conventionally designed, full girder version. In a further step, a numerical analysis of

selected optimized girder specimens is comprehensively discussed. The overall performance of the girders is finally evaluated and concluding remarks as well as suggestions for future research round off the paper.

2 | CONCRETE GIRDER OPTIMIZATION COMPETITION 2021/22

The Concrete Girder Optimization Competition (CGOC) was hosted by the Institute of Green Civil Engineering of the University of Natural Resources and Life Sciences Vienna in 2021/2022 with the overarching goal of bringing the fields of civil engineering and mathematical optimization closer together. The task was to find an optimized concrete girder design with minimal environmental impact under given design space dimensions and a set static system (compare with Figure 6 at the top), provided that the requirements of a predefined load-carrying capacity corresponding to a point load of 30 kN were met. The Global Warming Potential (GWP) was consulted as the parameter for evaluation (more details can be found in Section 8). In addition to the environmental performance, the structural performance in terms of manufacturability and determined load-carrying capacity were of interest. The kick-off of the CGOC launched in June 2021 during the 14th World Congress of Structural and Multidisciplinary Optimization (held online). The submission deadline was set with September 2021. Two designs were selected for experimental testing, with a workshop held in December 2021. The purpose of this workshop was to inform the participants about the boundary conditions of the experimental testing program as well as the respective limits of manufacturability, to allow for adaptions in regard to suitability for testing of the submitted designs. After a resubmission of the designs in February 2022, the experiments were finally conducted in May 2022, with the results presented in the following sections.

3 | DESIGN A

3.1 | Optimization strategy

The aim of submitter group A was to find a truss-like layout, with compressive forces transmitted by concrete-only and tensile forces by pure steel elements. The latter would be ideally realized in the form of external reinforcement bars, yet due to the lack of knowledge within the submitter group A, it was decided to go for an optimized reinforced concrete layout with conventional internal reinforcement bars. With this chosen approach in mind, submitter group A explored several established topology optimization procedures. Attempts to apply concurrent topology optimization of concrete and embedded reinforcement bars using nonlinear analysis based on previous research,[15,16] for example, did not yield satisfactory results. The relatively low volume of concrete within the slender design domain of the competition posed one of the bigger challenges when wanting to apply material nonlinear analysis of intermediate designs, that is, when the topology is still evolving and the domain is occupied by semi-dense material. As an alternative, initial design concepts were generated by a truss-based sizing and topology optimization equation, accommodating separate stress limits and CO_2 costs for tensile and compressive members, following the work of Achtziger.[17] The objective was to minimize the CO_2 weight associated with the amount of concrete and steel within the girder design. The volume of material was controlled by varying the areas of the cross sections of concrete and steel members while maintaining force equilibrium in the structure. The design variables for the given formulation comprised thus of the cross-sectional areas of the concrete and steel members, denoted $\mathbf{a}_c$ and $\mathbf{a}_s$, as well as the internal forces in each member carried by concrete and steel, denoted $\mathbf{q}_c$ and $\mathbf{q}_s$. The set of available bars was defined using a common "ground structure" parameterization, see for example, Bendsoe and Sigmung.[18] Constraints were imposed on the maximum stresses in tension and compression for both utilized materials. This lead to the linear programming formulation as found in Equation (1).

$$\mathbb{P} = \begin{cases} \min\limits_{\mathbf{a}_c,\mathbf{q}_c,\mathbf{a}_s,\mathbf{q}_s} & \sum\limits_{i}^{n} \left(w_c^i \rho_c^i a_c^i l_c^i + w_s^i \rho_s^i a_s^i l_s^i \right) \\ \text{subject to} & \begin{cases} \mathbf{B}\mathbf{q}_c + \mathbf{B}\mathbf{q}_s = \mathbf{f}_{ext} \\ \sigma_{min}^c \mathbf{I}\mathbf{a}_c - \mathbf{I}\mathbf{q}_c \le 0 \\ \sigma_{min}^s \mathbf{I}\mathbf{a}_s - \mathbf{I}\mathbf{q}_s \le 0 \\ -\sigma_{max}^c \mathbf{I}\mathbf{a}_c + \mathbf{I}\mathbf{q}_c \le 0 \\ -\sigma_{max}^s \mathbf{I}\mathbf{a}_s + \mathbf{I}\mathbf{q}_s \le 0 \\ \mathbf{a}_s \ge 0,\ \mathbf{a}_c \ge 0 \end{cases} \end{cases} . \quad (1)$$

In the objective of $\mathbb{P}$, subscripts "c" and "s" denote concrete and internal steel reinforcement, respectively; superscript "i" denotes a certain bar within the ground structure; w is the amount of CO_2 emitted per mass of raw material with the respective values taken as defined by the competition's rules (more details on the environmental analysis can be found in Section 8); ρ represents the mass density; l denotes the length of the bars and n the number of potential bars in the ground structure.

Equilibrium is imposed by projecting the bar forces to global coordinates using the matrix **B** and equating to the external loads $\mathbf{f}_{ext}$. In general, each bar should satisfy four stress limits: σ^c_{min}, σ^s_{min}, σ^c_{max} and σ^s_{max}. In this presented specific implementation, layouts with tensile steel and compressive concrete members were aimed for, therefore imposing $\sigma^c_{max} = \sigma^s_{min} = 0$. Finally, **I** stands for the identity matrix. Due to the necessary optimality conditions, the problem formulation (1) leads to fully stressed designs, that is, designs for which all bars with nonzero cross-sectional areas reach the allowable stress limit.

To better understand the effect of grid resolution of the ground structure on the optimal topology and objective value, a series of optimizations was executed with various levels of grid resolution. These varying ground structures consist of all possible nonoverlapping connections between the nodes of a regular mesh with rectangles with 20 nodes over the length of the domain and 2, 3, 4 or 5 nodes over the height. The outcomes are summarized in Figure 1, where $W_{structure}$ represents the structural weight and W_{CO_2} the total mass of CO_2 emissions. The black and grey bars represent the optimal members for tension and compression, respectively, while the arrow shows the introduction point for the external load. The effect of self-weight was not considered within the optimization process, because its contribution was found to be negligible compared to the external load. The results show that refining the grid resolution leads to a reduction in structural weight and an overall lower total carbon footprint. It should be noted that the impact on the objective is relatively small, while the complexity of the layout increases substantially. Considering the ease of manufacturability, the design shown in Figure 1a was selected for further design exploration.

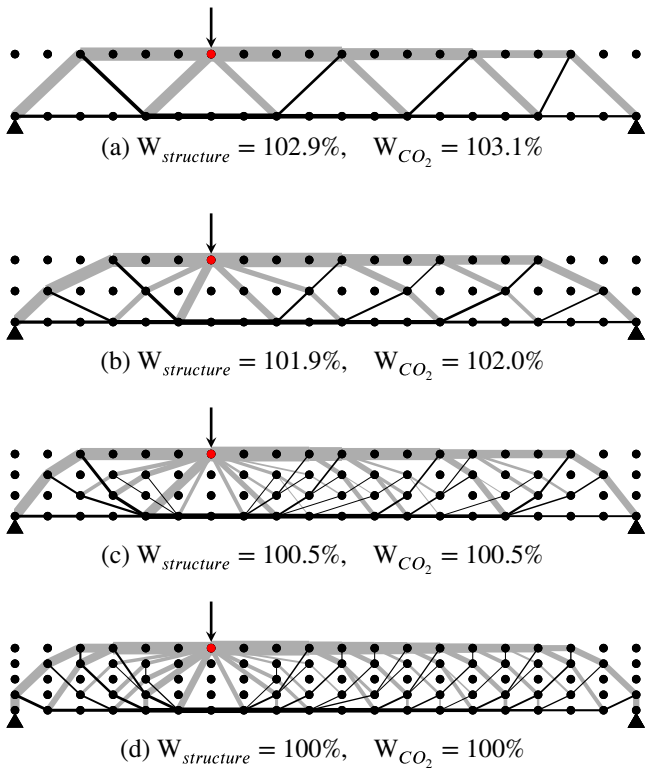

FIGURE 1 Optimal truss designs with various grid resolutions: (a) 20 × 2, (b) 20 × 3, (c) 20 × 4, (d) 20 × 5. The minimal amount of material is found with the finest grid and the relative increase in weight and CO_2 cost is indicated for each grid outlined by submitter group A (black—tension, grey—compression).

In the second design stage, the TopOpt plugin for Rhino-Grasshopper[19] was used to generate a continuum-based layout with distinct members in tension and compression. The theoretical background used within the plugin, as described by Aage et al.,[20] minimizes overall compliance subject to volume and cannot be used for detailed design as it does not include direct control over structural responses such as stresses and deflections. Nevertheless, it was used to assess whether it could be beneficial to adjust the locations of the nodes of the ground structure of the previously selected design from Figure 1a. The continuum optimization result obtained from the Grasshopper plugin for the girder is shown in Figure 2. Before detailed design iterations and further post-processing, slight modifications to the nodes' coordinates were made according to this newly obtained design proposal.

As a final step, to better understand the nonlinear structural response of the proposed optimal design, the software Vector2,[21] based on the Modified Compression Field Theory, was consulted. The latter assumes that cracked reinforced concrete can be modeled as a material with a newly defined stress–strain relation via averaging stresses and strains. The failure of the model was found to be governed by cracking of the concrete in joint regions of the girder. As such a complex failure mechanism is not covered by formulation (1), which only encompasses axial member stresses, a number of analysis-redesign iterations based on the nonlinear results were performed. The structural detailing of the final design is further explained below.

3.2 | Structural detailing and reinforcement strategy

Submitter group A pursued, as already outlined above, an internally reinforced truss-like concrete design. Formal building code requirements, such as set concrete covers or anchorage lengths, were not adhered to by submitter group A in a strict sense, as these would impose additional weight. Nevertheless, to avoid failure due to insufficient bond, anchorage of the longitudinal

FIGURE 2 Optimized continuum topology as generated by the TopOpt Grasshopper[19] plugin outlined by submitter group A (black—tension, hatched—compression).

reinforcement in the tensile members was ensured via extending the bars beyond the joints. Compression members were designed based on the optimum cross-sectional areas, with selected members being enlarged to avoid failure in buckling. In addition, the joints were designed by considering either an increased concrete area or embedding longitudinal steel elements at the joint block. Based on the nonlinear analyses that indicated local failure at the joints, vertical reinforcement elements were added at the joint blocks. The design and reinforcement layout of girder version *A*1 is outlined in Figure 6. It should be noted that the out-of-plane width of the girder designs was chosen with 60 mm based on that of the competition's design domain, simply because the submitter group of design A did not assume it to be open for optimization. The girder design *A*1 was produced according to submitted plans, with the small stirrup elements in the girder's joints realized as laser-cut stainless steel sheet elements. While for the diameter of the main tensile reinforcement 12 mm bars were chosen, 8 and 12 mm bars were implemented for the tensile struts.

To increase the output of the conducted test series, the hosts of the competition decided to adapt design *A*1 and produce an alternative, named *A*2. The underlying design alterations comprised of the integration of a stainless-steel fine mesh in and out-of-plane in compression areas as well as wrapping it around reinforcement bars in tension zones to effect equal crack distribution. Furthermore, the width of the chords and struts was increased and the placement of the reinforcement bars was specified so that the reinforcement bars were all placed on top of each other. The adapted girder design *A*2 is outlined in Figure 6.

4 | DESIGN B

4.1 | Optimization strategy

The submitter group of design B consulted strut-and-tie modeling (STM) as the design method of choice, as this method has been widely used in the design of reinforced concrete structures before and is implemented in various design codes.[22–25] In general, STM is based on a truss analogy with various feasible truss-like systems generated for the given design problem. The structural as well as economic performance is largely dependent on each individual model. In the present case, to systematically obtain accurate truss-like systems for the design problem of the competition, an STM method according to topology optimization based on previous research of submitter group B was adopted,[26,27] allowing for an automated generation of optimization-based strut-and-tie models (OPT-STM). The implemented method has proven successful in solving various design problems, where economic and safe designs were sought, compare with Xia et al.[28,29] In the initial optimization process, the classical Solid Isotropic Material with Penalisation (SIMP) topology optimization method according to Bendsoe and Sigmund[18] was applied. For a given structural design problem, this method finds the optimized material distribution by solving a compliance minimization problem as shown in Equation (2).

$$\begin{aligned} \text{minimize}: \quad & C(\boldsymbol{\rho}) = \mathbf{f}^{\mathrm{T}}\mathbf{u}(\boldsymbol{\rho}) \\ \text{subject to}: \quad & \mathbf{K}(\boldsymbol{\rho})\mathbf{u} = \mathbf{f} \\ & V(\boldsymbol{\rho}) \le \alpha \overline{V} \\ & \varepsilon \le \boldsymbol{\rho} \le 1 \end{aligned} \quad . \tag{2}$$

Here, C indicates the compliance of the structure. In the governing equation, $\mathbf{f}$, $\mathbf{u}$, and $\mathbf{K}$ represent the nodal force, displacement and stiffness matrix, respectively. By altering the density $\boldsymbol{\rho}$, which indicates the solid or void state of the structural elements, the optimized topology can be determined. To prevent the singularity of $\mathbf{K}$, a small value $\varepsilon = 0.0001$ is adopted as the lower limit of ρ. In addition, V and $\overline{V}$ denote the volume of the current topology and the total volume of the full domain. Finally, α is the predefined volume fraction.

For the development of the design for the competition, a finite element model with a mesh size of 5 mm and plane stress elements with four nodes was chosen. The volume of the optimized material distribution was limited to 30%. In order to avoid checker-board problems in the topology optimization,[30] a density filter according to Xia et al.[27] was applied. To consider manufacturability and the integration of a horizontally arranged reinforcement bar in the lower chord of the beam, the elements at the bottom of the design domain were chosen to remain non-design solid regions during the optimization process. The obtained material distribution, as illustrated in Figure 3a, could not be directly used as a strut-and-tie model. Topology extraction and also STM-based shape optimization procedures[26,27] were applied to transform the optimized topology into a suitable OPT-STM, as the automatically obtained truss-like structures from the

extraction process were unstable and required an axial-force equilibrium state. In the shape optimization process, the axial force equilibrium state of truss-like structures is quantified and subsequently used as an optimization constraint. The resulting model with force distribution, as shown in Figure 3b was subsequently used to determine the required steel and concrete cross sections of the ultimately submitted reinforced concrete design *B*1.

4.2 | Structural detailing and reinforcement strategy

A general design focus on the optimization of the steel arrangement can be found among scientific literature, as while the concrete often fills the entire design domain.[27,28] In the present case, both concrete and steel are designed based on the generated OPT-STM to further reduce material-related CO_2 emissions. The required reinforcement and concrete areas were calculated using the basic relation between force and stress.

Based on the results of the nonlinear finite element analysis performed by the competition hosts (compare with Section 7), showing lower ultimate capacity than the predicted design load, the compression and tension cross sections were further increased by the submitter group of design B. The structural detailing process also took into account manufacturing aspects, such as the uniform depth of concrete members, which was set to 40 mm and a consistent cross section of 8 mm of the used reinforcement bars. The ultimate optimization of girder version *B*1 is shown in Figure 3. Since external reinforcement was used, the related reduction in concrete mass led to an especially environmentally friendly design in terms of concrete reduction. The area of the main tensile reinforcement changed over the length, with a maximum of five reinforcement bars placed in the area of load introduction. Within every node leading toward the abutments, individual bars were bent upwards creating the steel ties. The detailed reinforcement layout is outlined in Figure 6. In order to obtain an adequate force transfer from the concrete struts to the steel ties, steel sheets were added in the joint areas, with the conceptual connection detail illustrated in Figure 4. The steel sheets were arranged to both provide confinement to the concrete and improve pullout capacity of the steel reinforcement bars from surrounding concrete. The connection of the reinforcement bars to each other and with the steel sheets was intended to be ensured by welding. The final design and reinforcement layout of girder version *B*1 is outlined in Figure 6.

As was the case for the submission of group A, the hosts of the competition decided to design a further concrete girder version, design *B*2 based on the submitted design *B*1. Similar to the changes from *A*1 to *A*2, design *B*2 included a stainless steel fine mesh in and out-of-plane in the compression areas in order to obtain an equal crack distribution. The girder design *B*2 is also outlined in Figure 6.

(a) SIMP topology of the investigated beam

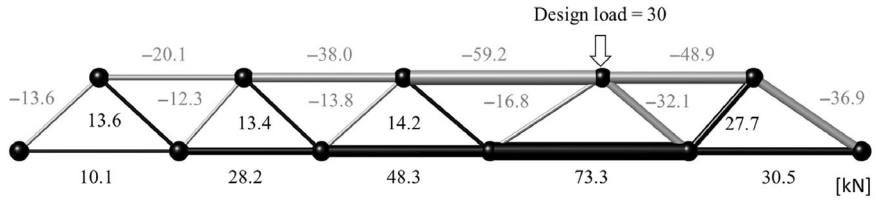

(b) Force distribution based on the obtained OPT-STM method under a design load of 30 kN (black - ties, grey - struts)

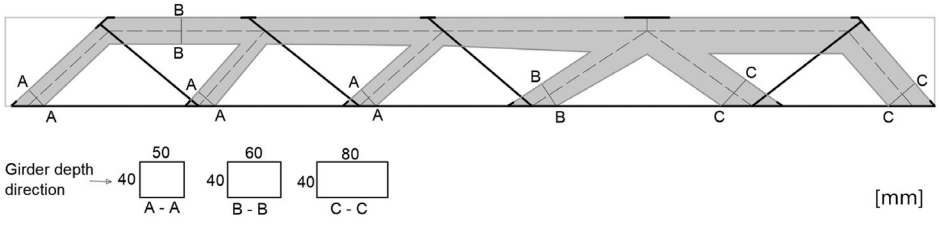

(c) Overall view of girder design *B*1 (black bold lines indicate external steel reinforcement bars and sheets)

FIGURE 3 Girder design *B*1 based on strut-and-tie modeling and topology optimization outlined by submitter group B (black—tension, grey—compression). (a) Solid Isotropic Material with Penalisation topology of the investigated beam. (b) Force distribution based on the obtained optimization-based STM method under a design load of 30 kN (black—ties, grey—struts). (c) Overall view of girder design *B*1 (black bold lines indicate external steel reinforcement bars and sheets).

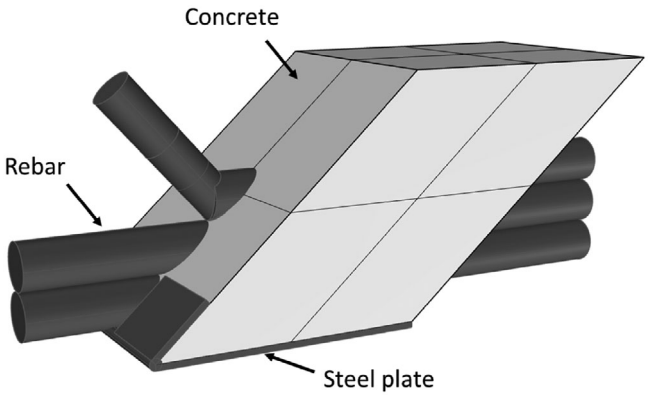

FIGURE 4 Conceptual design of a lower node region of the design outlined by submitter group B (dark grey—steel, light grey—concrete).

5 | FABRICATION

All specimens were produced and tested by the host of the competition. The formwork and installed reinforcement of girder versions *A* and *B* (exemplarily *A*2 and *B*2) are pictured in Figure 5. The girders were produced in lying position, with a formwork sheet serving as a base. For version *A*, the voids were realized as 3D filament extrusion-printed PLA elements, which were directly screwed onto the base sheet. The reinforcement bars were installed using spacers of varying dimensions. In the case of version *B*, a large number of formwork board elements had to be mitred. These were then cut in half, before slots, with a depth of 5 mm, were milled allowing for a penetration of the reinforcement elements right through the formwork. Window sealing tape prevented

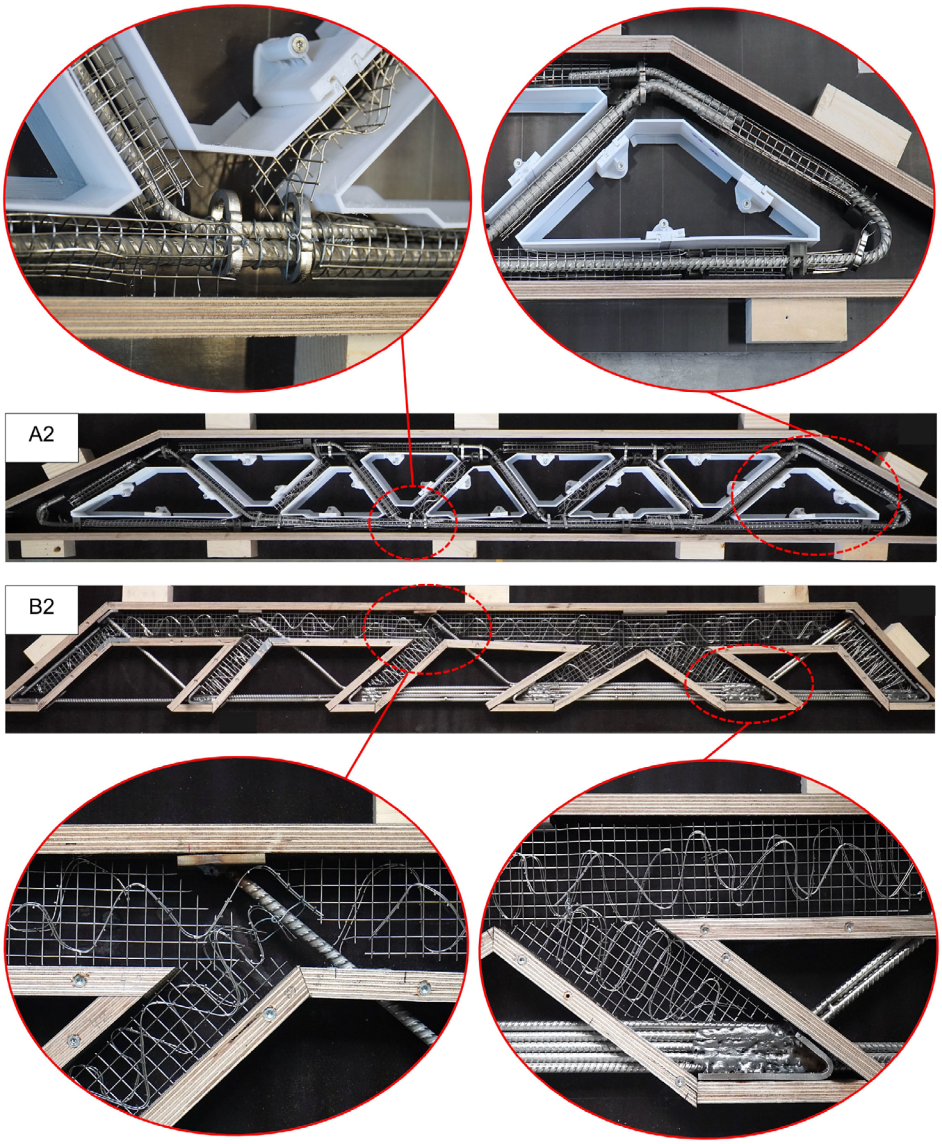

FIGURE 5 Top view of the formwork and reinforcement strategy with details (*A*2—top, *B*2—bottom).

leakage through the milled slots during concreting. The welded reinforcement bars and steel sheets were finally placed into the formwork in one piece. In a final step, the fine mesh was installed.

6 | EXPERIMENTAL INVESTIGATION

6.1 | Materials and test setup

For the concrete component of all girders a grouting mortar mixture[31] with a maximum grain size of 2 mm was used, with the latter being relevant due to the fine steel mesh width of only 10 mm. The concreting program consisted of following steps: Water addition (3.3 L per 25 kg bag of dry mixture), mixing in a drum mixer, concreting, coverage of specimens with plastic foil, storage at an ambient temperature of around 10°C and testing after a curing time of 33 to 34 days. In Table 1, the mean values of the experimentally determined concrete material parameters are summarized. The compression experiments on cubic/cylindrical and prismatic specimens with a loading rate of 0.001 mm/s were conducted according to ÖNORM EN 12390-3[32] and ÖNORM EN 1015-11,[33] respectively. The latter standard was also consulted in the case of flexural

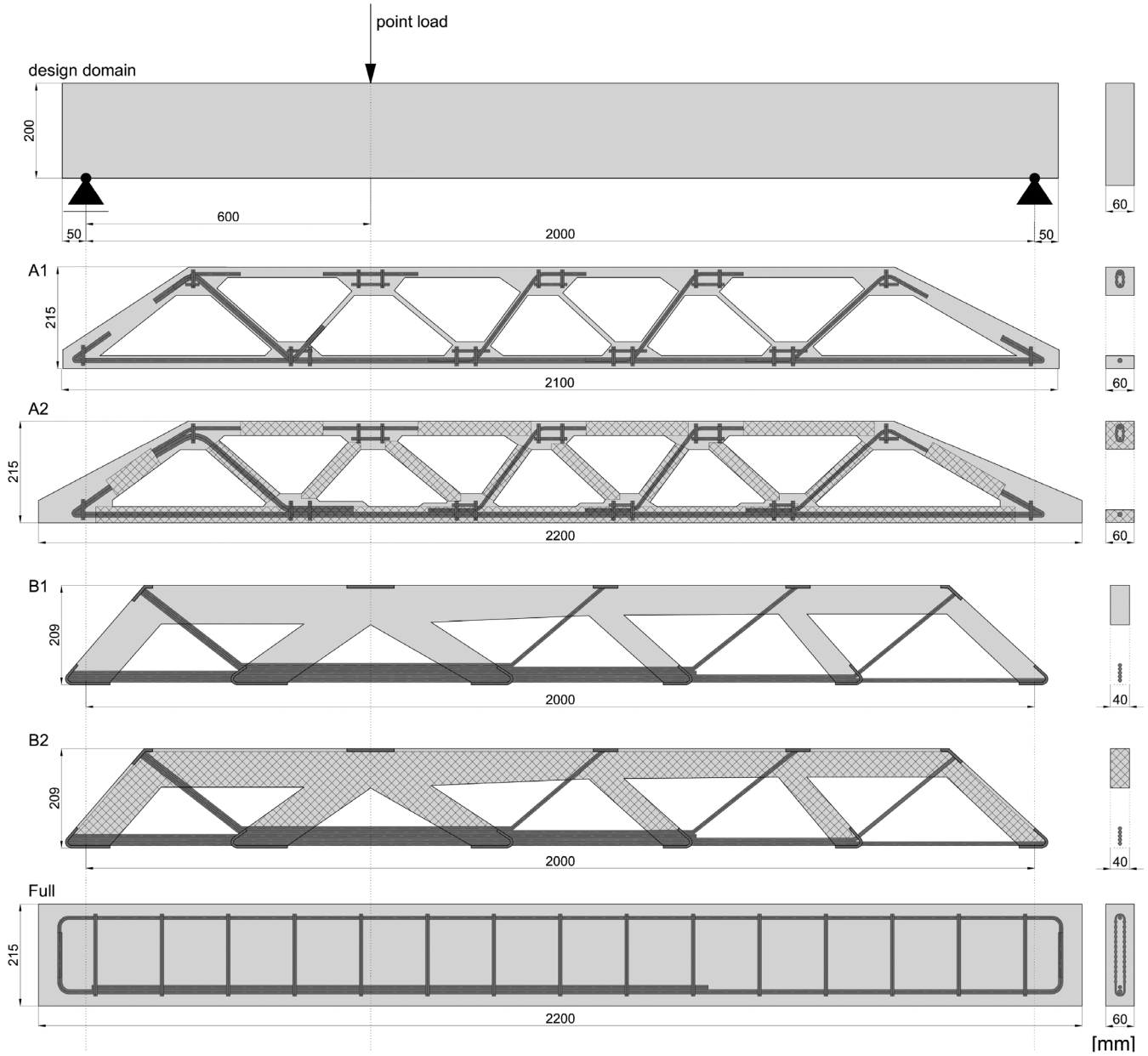

FIGURE 6 Design domain (top) and girder specimens with reinforcement layout (fine mesh—hatched areas, reinforcement bars, laser-cut reinforcement elements) with cross sections.

TABLE 1 Material properties of the grouting mixture[31] as obtained by hardened concrete testing.

Description	Parameter	Unit	Specimen dimensions (mm)	Specimen count	Mean value
Cube compressive strength	$f_{cm,cube}$	MPa	150 × 150 × 150	4	87.6
Cylinder compressive strength	$f_{cm,cylinder}$	MPa	150 × 300	4	80.7
Prism compressive strength	$f_{cm,prism}$	MPa	40 × 40 × 40	18	87.3
Flexural tensile strength	f_{ftm}	MPa	160 × 40 × 40	9	8.8
Splitting tensile strength	f_{stm}	MPa	100 × 200	4	3.7
Young's modulus	E_{cm}	MPa	160 × 40 × 40	9	32,640

tension tests (loading rate of 0.003 mm/s). The Young's modulus tests were carried out on prismatic specimens according to ÖNORM EN 12390-13[34] (method B) using an extensometer. The splitting tensile strength was determined according to ÖNORM EN 12390-6.[35]

Due to the small or even inexistent concrete cover, stainless steel types 1.4571 and 1.4362 were used as stirrup reinforcement and main tensile bar reinforcement, respectively. Regarding the latter, a yield strength $f_{y,rebar}$ of approximately 690 MPa, a tensile strength $f_{t,rebar}$ of around 880 MPa and a Young's modulus $E_{y,rebar}$ of 155,000 MPa were determined. For the laser-cut steel sheets, a yield strength $f_{y,stirrup}$ of approximately 280 MPa, a tensile strength $f_{t,stirrup}$ of around 600 MPa and a Young's modulus $E_{y,stirrup}$ of 195,000 MPa were obtained. The above-outlined properties of the steel materials were determined in tensile tests, using strain gauges.

For comparison reasons, a full girder with a rectangular cross section, designed according to Eurocode 2[36] and pictured at the bottom of Figure 6, was produced and tested within the study. Due to the slimness of the girder, special stirrups, more precisely laser-cut from 4 mm stainless steel sheets, needed to be used. The diameter of the main tensile reinforcement bundle, also made of stainless steel, was either 8 or 10 mm.

The experiments were conducted using a servo-hydraulic testing machine. The static system was a single span girder with an asymmetrically applied point load as outlined at the top of Figure 6. The girders were placed on rotatable bolts and the point load was introduced by a vertically movable steel section. An external displacement transducer was installed at the area of load introduction to measure the deflection w while loading. The force F was directly measured by the load cell integrated within the testing machine.

6.2 | Load-displacement curves

The load-displacement (L-D) curves of the experiments are outlined in Figure 7. The highest load of just below

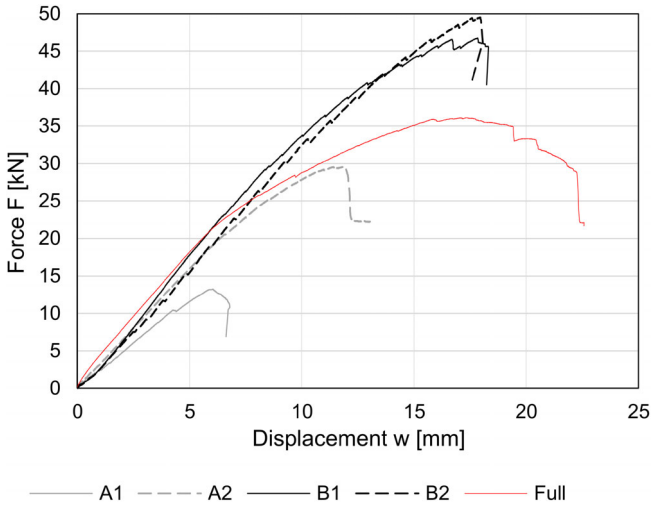

FIGURE 7 Load-displacement curves of the experiments.

50 kN was achieved by girder specimen *B*2, with the stiffness and load-carrying behavior of the original girder version *B*1 showing similar results. This similarity of the results is not the case for girder versions *A*1 and *A*2, with maximum loads of around 13 kN and just below 30 kN, respectively. The structural alterations made by the competition hosts showed greater effect as they activated load-carrying reserves, with the structural behavior explained into more detail in Section 6.3. The maximum load of the full girder version was around 36 kN. As the initially determined target load of the competition was 30 kN, girder version *A*2 obtained the best results from that aspect.

6.3 | Crack pattern and failure modes

The optical, contactless measurement method Digital Image Correlation (DIC) was used to assess the structural performance in more detail. Following settings were chosen: A subset size of 35 pixels, a step size of 7 pixels, a consistency threshold of 0.02, a confidence threshold of 0.05 and a strain filter size of 5 data points. The engineering

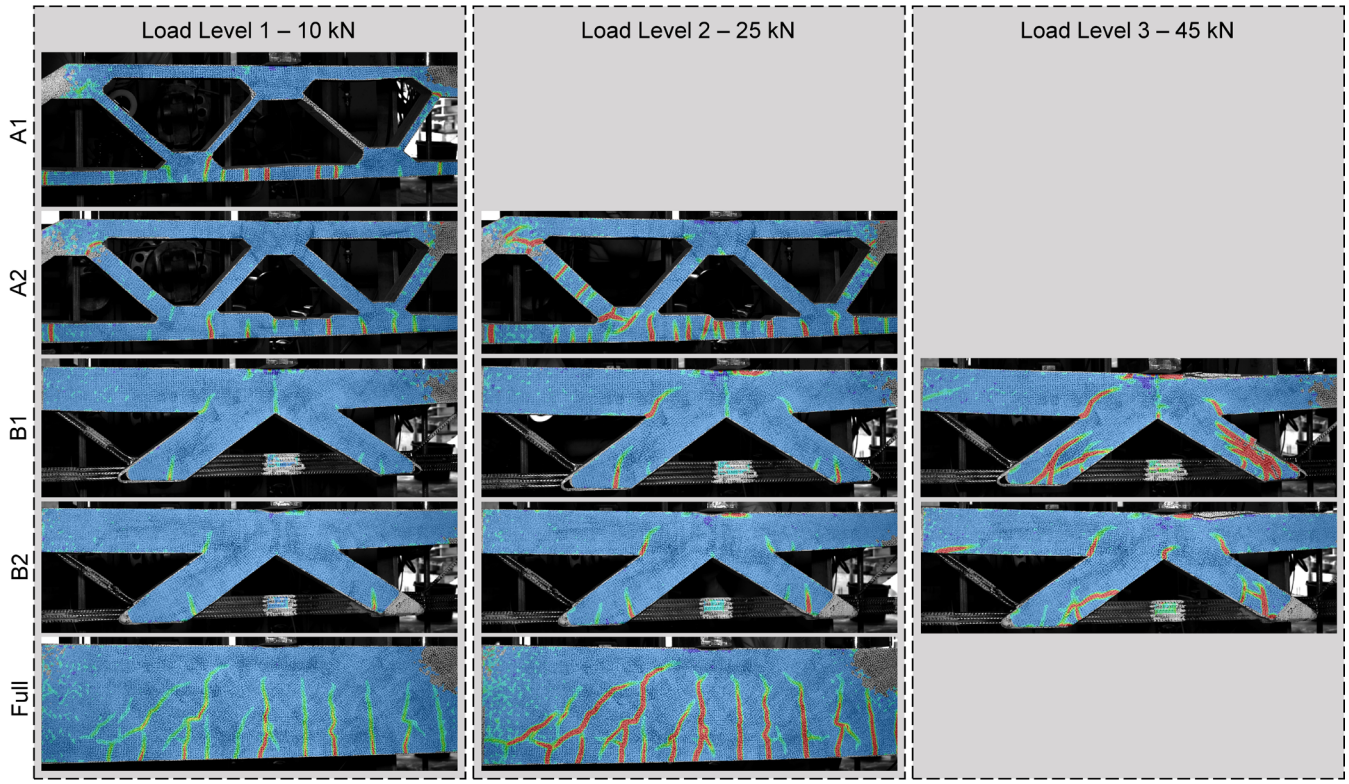

FIGURE 8 Principal strains of the various girder specimens at different load levels (red—maximum principal engineering strains of 1% or above, blue—zero strains).

strains were calculated and the strain distributions at different load levels obtained from post-processing are illustrated in Figure 8, allowing for an identification of cracking patterns. Three load levels were defined: Load Level 1 at 10 kN, Load Level 2 at 25 kN and Load Level 3 at 45 kN.

When analyzing Figure 8, one can detect that girder version *A*1 is characterized by significant separation cracks of the lower chord at Load Level 1. Just before failure, pronounced longitudinal-diagonal cracks appeared at the upper left compression-compression-tension node (not yet visible at Load Level 1). These cracks probably result from arising deviation forces in combination with high tensile forces within the adjacent tension tie, weakening the girder's node area and, subsequently, resulting in an abrupt failure. The same crack formation is recognizable for girder specimen *A*2 with the respective cracks growing at a comparatively higher load. In this case, the initiation of the longitudinal-diagonal cracks is already visible at Load Level 2. As the concrete width of the struts and chords was widened within *A*2 compared to *A*1, higher forces were transferred before failure.

In the case of *B*1 and *B*2, the lower connection area of the two compression struts and the longitudinal main bar reinforcement (load introduction area) showed growing visible vertical-diagonal cracks while loading. It can be assumed that these cracks develop due to the elongation of the main bar reinforcement, starting at low load levels and further propagating during the experiment. Further cracks, probably caused by the elongation of the bar reinforcement on opposite sides and leading to a drifting apart of the compression struts, are found in the corner areas of the voids, where the compression struts meet. Although *B*1 and *B*2 have similar looking L-D curves (Figure 7), the amount and intensity of cracks is visibly higher for *B*1, which is with high probability caused by the missing fine mesh.

Regarding girder version *Full*, typical bending tensile cracks appear during low load levels, later resulting in a critical shear crack further propagating into the compressive zone, indicating bending shear failure. Yielding of the stirrup or bar reinforcement was not able to be concluded from the DIC results, nevertheless, the strains in the compression zone of the concrete area could be measured clearly showing the reduction of its height at the point of load introduction. It has to be noted that, due to external influences, the first experimental test trial of girder version *Full* had to be stopped unplanned at a load level of around 20 kN and restarted once again. As a result, the transition from uncracked to cracked state is not recognizable in Figure 7, as the cracks have already formed in the first partial experimental trial of loading and only the second entire trial is displayed.

TABLE 2 Selected material properties for the numerical simulation.

Description	Value
Cube compressive strength f_{cu} [MPa]	87.6
Cylinder compressive strength f_c [MPa]	80.7
Tensile axiale strength f_t [MPa]	3.7
Young's modulus E [MPa]	32,640
Fracture energy G_f [N/m]	80
Strain at compressive strength (uniaxial) ε_c [−]	3.4
Poisson ratio μ	0.2
Specific material weight ρ [MN/m^3]	2.3

In terms of serviceability, exemplarily a load level of 15 kN can be considered in Figure 7, equalling 40% of the reference beam's ultimate load. Only a rather small scatter of the deflection values (between 4 and 5 mm or a deflection value of 1/500 and 1/400 in relation to the span length) of the tested girder specimens can be identified. Hence, the positive result of not having losses in terms of serviceability in the considered relevant area can be highlighted.

7 | NUMERICAL SIMULATION

7.1 | Methodology

The numerical analysis of reinforced concrete girders under consideration of material nonlinearity is already highly complex. Additional specific difficulties arise when applying such a method to structurally optimized concrete girders. Due to the organic shape of optimized concrete structures, for example, impairments in the discretization of concrete macro elements might be the result. An uneven distribution of finite elements can possibly lead to distorted elements, a higher computation time as well as convergence issues. In general, the input of such an unconventional, complex geometry makes the phase of preprocessing more time-consuming. The aim of the present study was to numerically re-simulate the conducted tests and to achieve satisfying alignment between peak loads as well as depict the respective failure modes. Based on the presented approach researchers can consult this publication for performing own numerical analyses on optimized concrete girders and estimate the load-carrying capacity before carrying out tests. Apart from that, the nonlinear numerical simulation was conducted in the course of the competition to assess the submitted designs, identifying early and unwanted failure modes, hence, serving as a tool and an additional round of optimization for the structural designs before experimental investigation. The girder versions $A2$ and $B1$ were selected for numerical analyses. The former was selected due to its more favorable load-carrying capacity and behavior in comparison to $A1$. As the girders $B1$ and $B2$ behaved rather similarly, girder version $B1$ without fine mesh was chosen for completion of the numerical investigation program, as girder version $A2$ already consisted of such a fine mesh. To do so, the software ATENA[37] was consulted, which is particularly suitable for the nonlinear analysis of reinforced concrete structures. In case of the main concrete bodies quadrilateral elements with a size of 1 cm and bi-linear interpolation functions were chosen. The reinforcement was modeled discrete with 1-dimensional elements. The slip at the end and beginning of the main reinforcement bars in the upper and lower chords of the specimens was set to be disabled, which corresponds with the hooked ends of the reinforcement bars in reality.

The nonlinear material modeling strategy of concrete was considered according to Pressmair et al.,[38] where the material properties obtained from testing (see Table 1) are taken as input parameters. The respective numerical material parameters are listed in Table 2. The selected material model *SBETA* as offered by the consulted software ATENA,[37] is characterized by the consideration of a nonlinear compression behavior, nonlinear fracture mechanics in tension, the inclusion of hardening and softening effects and the modeling of cracking among other numerical modeling concepts. A decisive parameter is the critical compressive displacement w_d, which is not only dependent on the material, but also on the failure mode, therefore ranging from 0.5 to 2 mm in the case of $A2$ and $B1$, respectively. For further details the reader is referred to Pryl and Červenka.[39] Other settings include a fixed crack model, an exponential tension softening type and a reduction of compression strength due to cracks set to 0.8. A bi-linear material model with hardening was chosen in case of the stirrup and reinforcement bar materials. Regarding reinforcement bond, a bond law according to Rabi et al.,[40] who highlight the generally lower bond strength that can be associated to stainless steel reinforcement comparable to equivalent carbon reinforcement steel, was defined.

The analysis was performed in 2D, with the supports defined as a combination of a horizontally sliding and a fixed support. In the first analysis step, the dead load of the system was applied, followed by a displacement of 0.05 mm per analysis step. The reaction and vertical deflection were directly monitored at the point of load introduction. The Newton–Raphson method served as solver, with the iteration number limit set to 300 steps. Other respective settings, such as tolerances, were adopted from the default settings offered by the consulted software.

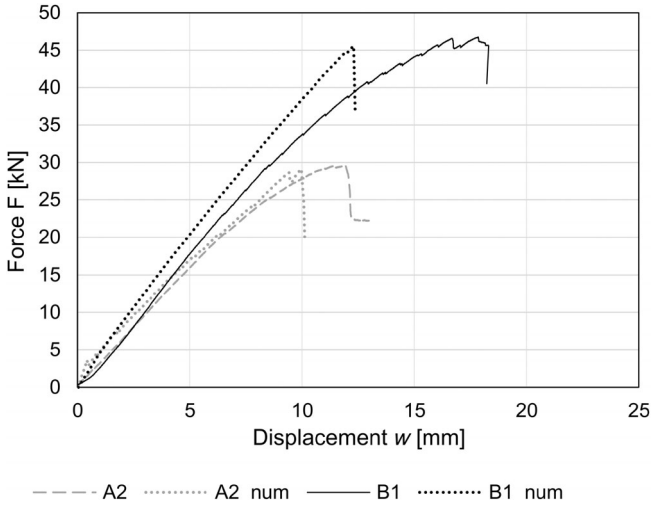

FIGURE 9 Experimental and numerical load-displacement curves of girder versions *A*2 and *B*1.

7.2 | Discussion of numerical results

The numerical L-D curves of girder version *A*2 and *B*1 are illustrated as dotted lines in Figure 9. The maximum load of the numerical simulation of *B*1 corresponds very well with the experimental result with a deviation of less than 5%. The failure of the compression zone within the load introduction area appeared in the numerical simulation as it did in the experiments, showing that the compressive-affine values, specifically the critical displacement w_d, had a high impact on the resulting L-D curve. Furthermore, the numerically obtained crack pattern agreed well with that of the experimental investigation. Nevertheless, the stiffness of the numerical simulation is significantly higher. In reality, the individual reinforcement bars are not only welded to each other, but also to the steel plates in the joint areas. To simulate this structural connection the authors pursued the following strategy: Due to their small size, the steel sheets were not modeled as macro elements, but rather several smaller reinforcement bars, simulating the fixed connection between sheets and bars. It must be assumed, that the precise effects of the welded girder joints on the overall system's compliance, possibly effected by small relative displacements between concrete and reinforcement material as well as the partial embedment of the reinforcement within the surrounding concrete, could not be accounted for in detail in the present study. The latter could be achieved via the development of a simulation strategy, accompanied by an experimental testing regime, which extends the scope of the present paper. Apart from that, it should also be noted that in contrast to the numerical analysis, a slip is detected within the experimental L-D curve at the beginning of loading until the entire structural system is activated and engaged within the load-carrying process.

In the case of *A*2, which was produced by adding fine mesh in specific regions, the experimental and numerical maximum loads match perfectly. In the axial direction of the reinforcement elements, the fine mesh was accounted for as an additional reinforcement area of the main stainless steel bars (approximately +10% each), while in lateral direction to the reinforcement bars it was not accounted for explicitly. The bond behavior shows a rather high sensitivity on the results, with further refinements and parameter studies possibly even leading to a better alignment between both curves. Last, it can be noted that while the transition from uncracked to cracked state is well visible in the case of the numerical analysis, this cannot be clearly detected within the experiments.

When comparing the deflection values of the numerical curves in Figure 9 at a load level of around 15 kN, a similar conclusion as it was the case for the experimental curves can be reached: The scatter of the deflection (between 3 and 4 mm) is rather low. Due to the fact that the experimental tests on the full girder had to be restarted and do not depict the transition from uncracked to cracked state, the authors refrained from including the numerical simulation of girder version *Full* within the following section due to the respective unsatisfactory data site.

The above-outlined results show that the numerical analysis of optimized concrete girders with novel reinforcement strategies is feasible, with the experimental and numerical maximum load-carrying capacity showing outstanding alignment. In order to better align the resulting stiffness of *B*1, further understanding of the unknown effects of the steel sheets on the overall girder's behavior would be necessary.

8 | ENVIRONMENTAL PERFORMANCE

The comparison of the gross concrete masses, the GWP of the concrete and reinforcement materials as well as the overall performance per girder specimen are outlined in Figure 10. The latter is defined by the division of the GWP by the maximum obtained testing load. For this evaluation, the production phase of the materials was considered (life cycle phases A1 to A3 according to ÖNORM EN 15840[41]). The consulted environmental data comprise the following sources: InformationsZentrum Beton GmbH[42] for concrete of a quality of C50/60 and Outokumpu Oyj[43] for stainless steel reinforcement. The girder version *Full* serves as the reference base for comparison. It can be shown that the concrete mass savings of all optimized girder specimens are significant and

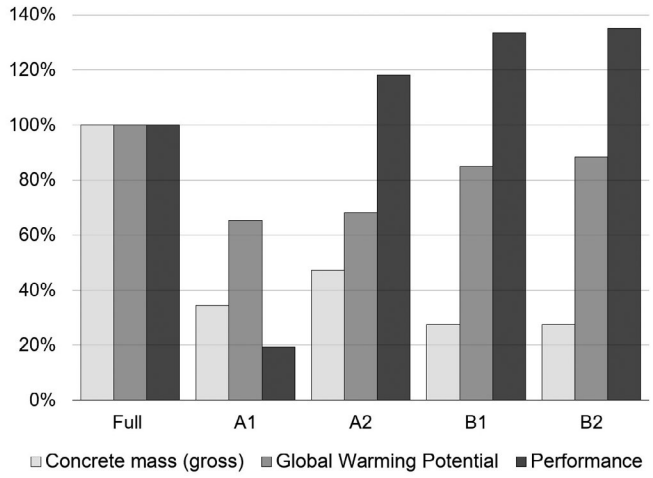

FIGURE 10 Comparison of the gross concrete masses (light grey bars, left), the Global Warming Potential (dark grey bars, center) and the performance (black bars, right) of the tested girder versions with the full concrete girder as reference.

larger than 50%, nevertheless, the GWP cannot be directly related to the concrete mass savings as this value is also dependent on the reinforcement mass. The reinforcement mass of the girder version *Full* amounts to 4.0 kg, increasing for girder versions *B*1 and *B*2 to 4.7 kg each and decreasing girder versions *A*1 and *A*2 to 3.3 and 3.0 kg, respectively. The share of the concrete mass regarding total GWP varies between 10% and 17% for the optimized girder versions and 36% for the full girder version. The fine mesh was considered within the evaluation of the environmental impact with a weight of 1.2 kg/m^2. Regarding girder versions *B*, about one third of the total reinforcement amount can be accounted to the 6 mm thick steel sheets at the ends of the reinforcement bars. Their thicknesses could probably be further reduced. The comparison of the performance in Figure 10 shows that the load-carrying capacity should also be considered, as not only masses are reduced but performance is increased. Design version *B*2, for example, shows a final performance increase of 35% in comparison to the full pendant, even though it is characterized by the comparatively highest stainless steel reinforcement mass.

9 | CONCLUSION

The present paper outlines the optimization, design, experimental investigation, numerical analysis and environmental performance assessment of two unconventional structurally optimized concrete design concepts. While one is internally reinforced with minimal concrete cover (girder design *A*), the other is designed with external reinforcement (girder design *B*), therefore reducing the concrete mass to a minimum. For both girder concepts, a version 1 and 2, the latter being additionally adapted with structural alterations, were investigated. For comparison reasons, a conventionally reinforced full girder was additionally designed, resulting in a total number of five girders tested (*A*1, *A*2, *B*1, *B*2 and *Full*). The entire research presented in this study is embedded in the framework of a competition hosted by the Institute of Green Civil Engineering at the University of Natural Resources and Life Sciences in Vienna, aiming at bringing the two fields of civil engineering and mathematical optimization closer together. The main findings are as following:

- Although the optimization approaches of the two investigated optimized girder design concepts are based on methods with comparable intentions, namely finding optimized strut-and-tie layouts, the final experimental results show a high variability. The results of group A are based on linear programming with limits on stresses and CO_2 emissions, whereas the ones of the group B are found via a strut-and-tie modeling method based on topology optimization. In theory, both approaches lead to adequate results of strut-and-tie models under the given boundary conditions, nevertheless, the structural interpretation of group B's optimized design led to a better overall outcome. This indicates that an adequate structural implementation of the "raw" optimization results is highly relevant to achieve satisfying results. Especially the results of *A*2 compared to *A*1 support this statement. Targeted changes in the structural detailing phase resulted in the load-carrying capacity of *A*2 being more than twice as high as that of *A*1.
- The greatest challenge within the structural interpretation process was the structural detailing of the joint connections. The steel sheet masses in nodal regions of girder version *B* are also responsible for a significant share of the overall GWP and appear to have still significant room for optimization. With regard to future research, more attention should therefore be paid to the development of strategies for joint design in the context of structurally optimized concrete girders.
- The externally reinforced girder version *B*, which is characterized by a comparatively stricter separation of concrete and reinforcement material in compression and tension zones, showed the highest performance measured in terms of environmental impact versus maximum load-carrying capacity. This result can be attributed to the fact that the structural failure mode that arose in the case of girder design concept *A* (likely due to a weakening caused by deviation forces in the compression-compression-tension node close to the support region) could not develop according to the reinforcement strategy of *B*. In addition to the outlined potential, such girder designs and/or uncommon

reinforcement concepts are accompanied by the need for a better understanding of their structural behavior. The numerical analysis, offering a base for predicting experiments beforehand, for example, outlined difficulty in capturing the inherent peculiarities in terms of system-specific compliance behavior of girder version *B*.

- The comparison of the environmental performance of the various concrete girders showed that the main impact can be traced back to the reinforcement and not to the concrete mass. This finding suggests that when developing resource-efficient concrete structures, the optimization—or rather minimization—of reinforcement should be assigned high priority in addition to concrete mass reduction. In this context, it should be noted, that this conclusion is also strongly based on the fact that stainless steel reinforcement was used in the present study. The weighting of the environmental impact shares would be different for conventional reinforcement, nevertheless show similar tendency.

The collaboration between experts in the fields of mathematical optimization and structural concrete engineering as outlined within the present publication led to successful results and perceptible learning effects on both sides, therefore once more highlighting the potential of optimized concrete girders to reduce the use of resources while maintaining or even increasing structural performance. The authors want to highlight that the findings and statements made within the publication are only suitable within the boundaries of the presented competition. A direct consideration of the serviceability limit state, for example, was not required; however, it should be accounted, for example, via a constraint of the deformation within an optimization process in future research. Furthermore, in terms of the environmental performance, the efforts in relation to the formwork geometry associated with labor and material demand was not considered, actually leading to higher values for the optimized girders in comparison to the full pendants. When neglecting further standard-specific requirements in terms of the full girder specimen design, additional material savings could be achieved in regard of the full pendant. The full girder can also be assumed to be more robust in terms of altering loading positions, keeping in mind that the investigated optimized designs are only valid for one single loading case. All in all, this demonstrates that a number of parameters outside of the boundaries of the competition, also having an influence on the results, exists. In the future, teaming up is especially recommended by the authors to accelerate the enhancement of resource-efficiency in the concrete construction sector and gain further insights into the topic. This statement does not limit itself to structural engineering and mathematics, but should also include other disciplines with regard to industrial manufacturability, prefabrication and implementation.

AUTHOR CONTRIBUTIONS

Nadine Pressmair: Conceptualisation, Methodology, Formal analysis, Project administration, Writing - Original draft, Writing - Review & editing, Experimental investigation, Software, Visualisation. **Yi Xia**: Methodology, Software, Writing - Original draft. **Hongfei Wu**: Software, Visualisation. **Matthijs Langelaar**: Conceptualisation, Methodology, Writing - Review & editing. **Max A. N. Hendriks**: Conceptualisation, Methodology, Writing - Review & editing. **Ahmad Majdouba**: Methodology, Formal analysis, Writing - Original draft. **Mihir Mogra**: Methodology, Software. **Hezi Grisaro**: Formal analysis, Writing - Original draft. **Oded Amir**: Conceptualisation, Methodology, Formal analysis, Writing - Original draft. **Benjamin Kromoser**: Research strategy, Conceptualisation, Supervision, Writing - Review & editing, Funding acquisition.

ACKNOWLEDGMENTS

Thank has to be granted to Dr. Mathias Hammerl, Dr. Matthias Braun, DI Peter Gappmaier, DI Roman Myna and the laboratory team of the Institute of Structural Engineering at the University of Natural Resources and Life Sciences in Vienna for their support during the experiments. Furthermore, regarding assistance in linguistic refinement, thank is expressed to Dr. Sara Reichenbach.

FUNDING INFORMATION

This research did not receive any specific grant from funding agencies in the public, commercial or not-for-profit sectors.

CONFLICT OF INTEREST STATEMENT

The authors declare that they have no known competing financial interests or personal relationships that could have appeared to influence the work reported in this paper.

DATA AVAILABILITY STATEMENT

The data that support the findings of this study are available from the corresponding author upon reasonable request.

ORCID

Nadine Pressmair https://orcid.org/0000-0003-3711-6974

Benjamin Kromoser https://orcid.org/0000-0003-3416-8146

REFERENCES

1. Andrew RM. Global CO_2 emissions from cement production, 1928–2018. Earth Syst Sci Data. 2019;11:1675–1710. https://doi.org/10.5194/essd-11-1675-2019
2. CO2-earth. Global caron emissions. 2021 Available from: https://www.co2.earth/global-co2-emissions
3. Nature. Concrete needs to lose its colossal carbon footprint. Nature. 2021; Available from: https://www.nature.com/articles/d41586-021-02612-5
4. Kromoser B. Betonkalender 2021: Fertigteile; Integrale Bauwerke - III Ressourceneffizientes Bauen mit Betonfertigteilen. Vienna: Ernst & Sohn GmbH; 2021.
5. Stoiber N, Kromoser B. Topology optimization in concrete construction: a systematic review on numerical and experimental investigations. Struct Multidiscipl Optim. 2021;64(4):1725–49. https://doi.org/10.1007/s00158-021-03019-6
6. Liang Q, Xie Y, Steven G. Generating optimal strut-and-tie models in prestressed concrete beams by performance-based optimization. ACI Struct J. 2001;98:226–32.
7. Ali MA, White RN. Automatic generation of truss model for optimal design of reinforced concrete structures. ACI Struct J. 2001;98(4):431–42. https://doi.org/10.14359/10286
8. Gaynor Andrew T, Guest James K, Moen Cristopher D. Reinforced concrete force visualization and design using bilinear truss-continuum topology optimization. J Struct Eng. 2013;139(4):607–18. https://doi.org/10.1061/(ASCE)ST.1943-541X.0000692
9. Mergos PE. Contribution to sustainable seismic design of reinforced concrete members through embodied CO_2 emissions optimization. Struct Concr. 2018;19(2):454–62. https://doi.org/10.1002/suco.201700064
10. Zhang X, Zhang X. Sustainable design of reinforced concrete structural members using embodied carbon emission and cost optimization. J Build Eng. 2021;44:102940. https://doi.org/10.1016/j.jobe.2021.102940
11. Smarslik M, Mark P. Hybrid reinforcement design of longitudinal joints for segmental concrete linings. Struct Concr. 2019;20(6):1926–40. https://doi.org/10.1002/suco.201900081
12. Gaganelis G, Mark P. Downsizing weight while upsizing efficiency: an experimental approach to develop optimized ultra-light UHPC hybrid beams. Struct Concr. 2019;20(6):1883–95. https://doi.org/10.1002/suco.201900215
13. Galmarini A, Locher D, Marti P. Predicting the responses of reinforced concrete slab strips subjected to axial tension and transverse load - a competition. Struct Concr. 2015;16(2):172–83. https://doi.org/10.1002/suco.201400097
14. Barros J, Sanz B, Kabele P, Yu RC, Meschke G, Planas J, et al. Blind competition on the numerical simulation of steel-fiber-reinforced concrete beams failing in shear. Struct Concr. 2021;22(2):939–67. https://doi.org/10.1002/suco.202000345
15. Amir O. A topology optimization procedure for reinforced concrete structures. Comput Struct. 2013;114:46–58. https://doi.org/10.1016/j.compstruc.2012.10.011
16. Shakour E. Topology optimization of reinforced concrete elements using continuum damage models. Haifa, Israel: Technion – Israel Institute of Technology; 2018.
17. Achtziger W. Truss topology optimization including bar properties different for tension and compression. Struct Optim. 1996;12(1):63–74. https://doi.org/10.1007/BF01270445
18. Bendsoe MP, Sigmund O. Topology optimization: theory, methods and applications. Heidelberg: Springer Science & Business Media; 2003.
19. Aage N, Sigmund O, Amir O, Maier D, Søndergaard A. TopOpt for Grasshopper. 2014 Available from: https://www.grasshopper3d.com/group/topopt
20. Aage N, Amir O, Clausen A, Hadar L, Maier D, Søndergaard A. Advanced topology optimization methods for conceptual architectural design. Advances in architectural geometry 2014. Springer; 2015. p. 159–79. https://adk.elsevierpure.com/da/publications/advanced-topology-optimization-methods-for-conceptual-architectur
21. Vecchio FJ, Collins MP. The modified compression-field theory for reinforced concrete elements subjected to shear. ACI J. 1986;83(2):219–31.
22. American Concrete Institute (ACI). Building code requirements for structural concrete and commentary. Farmington Hills, MI: ACI Committee 318-14; 2008.
23. fib (International Federation for Structural Concrete). fib model code for concrete structures 2010. Lausanne, Switzerland: Ernst & Sohn, Wiley; 2013.
24. American Association of State Highway Officials and Transportation (AASHTO). LRFD bridge design specifications. 7th ed. Washington, DC: AASHTO; 2014.
25. European Committee for Standardization (CEN). Eurocode 2: design of concrete structures-part 1-1: general rules and rules for buildings. 2017.
26. Xia Y, Langelaar M, Hendriks MA. A critical evaluation of topology optimization results for strut-and-tie modeling of reinforced concrete. Comput-Aided Civ Inf. 2020;35(8):850–69. https://doi.org/10.1111/mice.12537
27. Xia Y, Langelaar M, Hendriks MA. Automated optimization-based generation and quantitative evaluation of strut-and-tie models. Comput Struct. 2020;238:106297. https://doi.org/10.1016/j.compstruc.2020.106297
28. Xia Y, Langelaar M, Hendriks MA. Optimization-based three-dimensional strut-and-tie model generation for reinforced concrete. Comput-Aided Civ Inf. 2021;36(5):526–43. https://doi.org/10.1111/mice.12614
29. Xia Y, Langelaar M, Hendriks MA. Optimization-based strut-and-tie model generation for reinforced concrete structures under multiple load conditions. Eng Struct. 2022;266:114501. https://doi.org/10.1016/j.engstruct.2022.114501
30. Sigmund O, Petersson J. Numerical instabilities in topology optimization: a survey on procedures dealing with checkerboards, mesh-dependencies and local minima. Struct Optim. 1998;16(1):68–75. https://doi.org/10.1007/BF01214002
31. Sika GmbH. Data Sheet SikaGrout®-312; 2021. Available from: https://aut.sika.com/dms/getdocument.get/1f76fade-e164-4715-b945-a2eba3e6aebf/sikagrout_-312.pdf
32. OENORM EN 12390-3. Testing hardened concrete - part 3: compressive strength of test specimens. Vienna, Austria: Austrian Standards Institute; 2019.
33. OENORM EN 1015-11. Methods of test for mortar for masonry, part 11: determination of flexural and compressive strength of hardened mortar. Vienna, Austria: Austrian Standards Institute; 2020.
34. OENORM EN 12390-13. Testing hardened concrete, part 13: determination of secant modulus of elasticity in compression. Vienna, Austria: Austrian Standards Institute; 2021.
35. OENORM EN 12390-6. Testing hardened concrete, part 6: tensile splitting strength of test specimens. Vienna, Austria: Austrian Standards Institute; 2010.

36. OENORM EN 1992-1-1. Eurocode 2: Design of concrete structures - part 1–1: general rules and rules for buildings. Vienna, Austria: Austrian Standards Institute; 2015.
37. ATENA Cervenka Consulting. ATENA | Cervenka consulting; 2022. Available from: https://www.cervenka.cz/products/atena/
38. Pressmair N, Brosch F, Hammerl M, Kromoser B. Non-linear material modelling strategy for conventional and high-performance concrete assisted by testing. Cem Concr Res. 2022; 161:106933. https://doi.org/10.1016/j.cemconres.2022.106933
39. Pryl D, Červenka J. ATENA program documentation part 11 - troubleshooting manual. 2020 Available from: https://www.cervenka.cz/assets/files/atena-pdf/ATENA-Troubleshooting.pdf
40. Rabi M, Cashell KA, Shamass R, Desnerck P. Bond behaviour of austenitic stainless steel reinforced concrete. Eng Struct. 2020; 221:111027. https://doi.org/10.1016/j.engstruct.2020.111027
41. OENORM EN 15804. Sustainability of construction works - environmental product declarations - core rules for the product category of construction products. Vienna, Austria: Austrian Standards Institute; 2012.
42. InformationsZentrum Beton GmbH. Umweltproduktdeklaration - Beton Der Druckfestigkeitsklasse C50/60; 2018. Available from: https://www.beton.org/fileadmin/beton-org/media/Dokumente/PDF/Wissen/Beton-Bautechnik/Nachhaltigkeit/Beton_der_Druckfestigkeitsklasse_C_5060.pdf#
43. Oyj O. Environmental product declaration - stainless steel rebar. 2019 Available from: https://www.outokumpu.com/en/sustainability/sustainable-solutions/environmental-product-declarations

AUTHOR BIOGRAPHIES

Nadine Pressmair, Institute of Green Civil Engineering, University of Natural Resources and Life Sciences, Vienna, Austria.
Email: nadine.pressmair@boku.ac.at

Yi Xia, School of Civil Engineering, Chongqing University, Chongqing, China.
Email: yi_xia@cqu.edu.cn

Hongfei Wu, School of Civil Engineering, Chongqing University, Chongqing, China.
Email: hongfei_wu_cqu@163.com

Matthijs Langelaar, Faculty of Mechanical, Maritime and Materials Engineering, Delft University of Technology, Delft, The Netherlands.
Email: m.langelaar@tudelft.nl

Max A. N. Hendriks, Faculty of Civil Engineering & Geosciences, Delft University of Technology, Delft, The Netherlands.
Email: m.a.n.hendriks@tudelft.nl

Ahmad Majdouba, Faculty of Civil and Environmental Engineering, Technion – Israel Institute of Technology, Haifa, Israel.
Email: majdouba@campus.technion.ac.il

Mihir Mogra, Faculty of Civil and Environmental Engineering, Technion – Israel Institute of Technology, Haifa, Israel.
Email: mihirmogra@campus.technion.ac.il

Hezi Grisaro, Faculty of Civil and Environmental Engineering, Technion – Israel Institute of Technology, Haifa, Israel.
Email: hezi@technion.ac.il

Oded Amir, Faculty of Civil and Environmental Engineering, Technion – Israel Institute of Technology, Haifa, Israel.
Email: odedamir@technion.ac.il

Benjamin Kromoser, Institute of Green Civil Engineering, University of Natural Resources and Life Sciences, Vienna, Austria.
Email: benjamin.kromoser@boku.ac.at

How to cite this article: Pressmair N, Xia Y, Wu H, Langelaar M, Hendriks MAN, Majdouba A, et al. Bridging the gap between mathematical optimization and structural engineering: Design, experiments and numerical simulation of optimized concrete girders. Structural Concrete. 2023. https://doi.org/10.1002/suco.202201096